Fuel 307 (2022) 121910

Contents lists available at ScienceDirect

Fuel

journal homepage: www.elsevier.com/locate/fuel

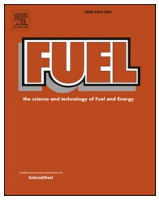

Full Length Article

Partially premixed combustion of hydrotreated vegetable oil in a diesel engine: Sensitivity to boost and exhaust gas recirculation

Jacek Hunicz [a], Maciej Mikulski [b,*], Pravesh Chandra Shukla [c], Michał S. Gęca [a]

[a] Lublin University of Technology, Faculty of Mechanical Engineering, Nadbystrzycka 36, 20-618 Lublin, Poland
[b] University of Vaasa, School of Technology and Innovation, Wolffintie 34, FI-65200 Vaasa, Finland
[c] Indian Institute of Technology Bhilai, Department of Mechanical Engineering, Raipur, India

ARTICLE INFO

Keywords:
Hydrotreated vegetable oil
Multi-pulse injection
Exhaust gas recirculation
Boost
Partially premixed compression ignition
Optimisation

ABSTRACT

Hydrotreated vegetable oil (HVO) has potential to emerge as an alternative fuel to mineral diesel due to its favourable properties. The present study investigated HVO under partially premixed compression ignition combustion mode with boost-exhaust gas recirculation (EGR) and also in conventional combustion mode. Single-cylinder engine tests focused on optimising a single representative operating point in the middle of the engine operating envelope. The optimisation focused on the trade-off between NO_X and particulate matter, as the adopted multi-pulse strategy provides stable combustion onset independently of the cylinder mixture conditions. Sensitivity in emissions comes from large differences in the early, premixed combustion phase. Air-path optimized HVO combustion favours higher EGR rates (25 % vs. 20 %) and lower boost pressures than diesel (130 kPa vs 165 kPa). At such conditions HVO has 1.5 percentage points higher indicated thermal efficiency (43.5 %) than diesel. At the same time, HVO yields an ultra-low particulate level (0.055 g/kWh) and engine-out NO_X emissions are 46 % better than optimised diesel combustion. Together with a 37 % reduction in total hydrocarbon emissions, the elimination of aromatics also provides an additional incentive for HVO.

1. Introduction

The diesel engine has been the prime mover for global road transport over the last century. Despite its aggravating reputation, thorough life cycle analyses prove diesel propulsion has a smaller carbon footprint than its advocated battery-electric successor in most scenarios [1]. The real constraints of energy–density and lengthy fleet renewal intervals mean that diesel engines will remain the backbone of heavy commercial vehicles and marine transport in the foreseeable future.

Gradual replacement of fossil fuels with their renewable counterparts is an important part of an integrated approach towards transport sustainability. Still, the biofuel share in the global energy consumption by the transport sector is currently as low as 4 % [2]. Fatty acid methyl esters (FAME) produced by transesterification remain a major alternative for diesel fuel (DF) in compression ignition (CI) engines. FAME has currently a 32 % share in the worldwide biofuel market [2]. However, its commercial use is limited due to its deleterious effects on fuel injection systems, poor oxidation stability [3] and elevated oxides of nitrogen (NO_X) emissions [4]. Additionally, FAME's feedstock dependency on edible oils poses challenges with respect to food production and associated land use intensification.

Alternatively, hydrotreated vegetable oil (HVO) has potential to emerge as a better diesel substitute [5]. HVO is produced by hydroprocessing bio-oils, where broken-down triglycerides undergo decarboxylation, decarbonylation and hydrodeoxygenation, yielding paraffinic hydrocarbons [6]. The ability to produce HVO from non-edible feedstock benefits the well-to-wheel carbon dioxide (CO_2) emissions, which reportedly can be reduced by 90 % when compared to DF [1]. HVO has similar properties to DF, so its application is not limited to small-scale blends, as with FAME. Thus, HVO can fully utilise the existing fuel infrastructure and is currently available as stand-alone, drop-in fuel for diesel at over 500 filling stations in Europe and North America [1].

HVÓs inherent properties provide benefits in terms of mixture formation, better combustion and emission mitigation in diesel engines. HVÓs density and viscosity are both lower than DF́s. These properties, combined with a much flatter distillation curve and an end of distillation point 50 °C lower, support spray propagation and mixture formation. Hulkkonen et al. [7] performed comparative studies of spray parameters of DF and HVO in a constant volume chamber. It was observed that HVO's penetration distance was slightly shorter, while spray cone angle

* Corresponding author.
E-mail address: maciej.mikulski@uwasa.fi (M. Mikulski).

https://doi.org/10.1016/j.fuel.2021.121910
Received 28 April 2021; Received in revised form 17 August 2021; Accepted 2 September 2021
Available online 8 September 2021

Nomenclature

AHC	Aromatic hydrocarbon
CA50	CAD value for 50 % heat release
CAD	Crank angle degree
CDC	Conventional diesel combustion
CHR	Cumulative heat release
CI	Compression ignition
CN	Cetane number
CO	Carbon monoxide
CO_2	Carbon dioxide
DF	Diesel fuel
EGR	Exhaust gas recirculation
FAME	Fatty acid methyl esters
FTIR	Fourier transform infrared
HRR	Heat release rate
HVO	Hydrotreated vegetable oil
IMEP	Indicated mean effective pressure
ISFC	Indicated specific fuel consumption
ITE	Indicated thermal efficiency
MAP	Manifold absolute pressure
MFB	Mass fraction burnt
NO_X	Oxides of nitrogen ($NO + NO_2$)
PM	Particulate matter
PPCI	Partially premixed compression ignition
SoI	Start of injection
SoI_m	Start of injection (main injection)
SoI_p	Start of injection (pilot injection)
TDC	Top dead centre
THC	Total hydrocarbon
UHC	Unburnt hydrocarbons
λ	Excess air ratio (lambda)

was up to 2° wider. HVÓs droplet velocities at the early stage of injection were observed to be higher. Bohl et al. [8] confirmed these observations in their study, underlining that HVO produces a higher premixed charge with lower energy density. Cheng et al. [9] found similar results, supporting their macroscopic spray image analysis with a dedicated one-dimensional spray model. Notably, all these works conclude that the differences between DF and HVO, in terms of spray formation, are rather small when the net effect on combustion is considered.

On the other hand, HVO and DF are chemically different. Whereas DF has a complex paraffinic-olefin-aromatic structure, HVO is composed solely of simple paraffinic hydrocarbons. This underpins HVÓs very high cetane number, which is typically 69–75 [10]. Such a high cetane number affects auto-ignition delay and provides smoother heat release during HVO combustion [11]. Alkhayat et al. [12] reported 45 % shorter ignition delay for HVO vs. DF. After decoupling physical and chemical processes, they concluded that the result was equally attributable to spray formation and cetane number (CN) at nominal engine operating conditions. However, at elevated in-cylinder temperatures, the reduction in physical delay was greater than the reduction in chemical delay. Experiments in a constant volume chamber by Marasri et al. [13] showed that under low bulk temperatures, where auto-ignition delay typically is long, HVO provides higher heat release rate (HRR) than DF.

Large-scale testing of HVO was conducted by Helsinki Region Transport, Neste Oil, Proventia Emission Control and VTT Technical Research Centre of Finland [14]. The vast study used a 30 % HVO blend with DF for long-term tests on the fleet of approximately 300 buses with Euro IV engines. The test demonstrated an improvement in emission factors and did not indicate any of the reliability issues associated with other biodiesels [15,16].

Detailed laboratory research of HVO in heavy-duty engines [10] provided quantitative emission results. This study [10] showed that using HVO instead of baseline DF provided the following emissions reductions: unburnt hydrocarbons (UHC) fell by 48 %; carbon monoxide (CO) by 28 %; NO_X by 10 %; and particulate matter (PM) by 28 %. Additionally, HVO did not produce any aromatics. Aatola et al. [17] evaluated HVO's average emission benefits using a heavy-duty engine without exhaust gas recirculation (EGR) at variable speed and load conditions. UHC, CO and smoke emissions were reduced by 31–35 % and NO_X was reduced by 5 % vs. DF.

Experiments with light-duty engines have also showed emissions benefits when using HVO instead of DF, but results are heavily dependent on engine type. Some studies report NO_X emissions reductions at unchanged PM levels, while in other cases the trade-off was reversed [18]. This ambiguity was explained by research of Sugiyama et al. [19], who found that the PM-NO_X trade-off was dependent on whether single-injection or split-injection fuelling strategy was used. For single injection, HVO ignited earlier with reduced HRR, which supported lower NO_X, but increased PM creation. For split injection, main combustion remained unchanged, but HVO's pilot fuel ignited earlier. With similar combustion characteristics, HVO's lower chemical propensity to create PM was the governing mechanism for less PM when using split injection. Wu et al. [20] performed a detailed investigation of PM emissions and found that, over the whole engine operating map, the particulate number was halved when HVO was compared to DF. Contrarily, Bortel et al. [21] indicated that particulate number is unaffected by HVO, although PM emission is reduced by 80 %. It should be noted that these results were achieved without exhaust aftertreatment, and using factory engine calibrations.

Finally, it should be noted that HVO provides about 4 % lower tank-to-wheels CO_2 emission when compared to DF [18,22]. This gives a higher hydrogen to carbon ratio as well as a higher degree of complete combustion, supporting oxidation of HC and CO to CO_2.

The discussed effects of HVO on emission and combustion lead to a general conclusion that HVO performs better in modern combustion systems with multi-pulse injection strategies. The above-cited comparative studies performed using standard engine-control maps indicated scope for greater HVO benefits by engine re-calibration to take advantage of the fueĺs properties.

Aatola et al. [17] investigated HVO re-calibration potential, assuming variable main injection timing, preceded by a fixed pilot injection. The start of injection (SoI) sweeps revealed variable PM-NO_X trade-offs at different speeds and engine loads. Importantly, when compared with DF, at all conditions HVO produced 30–40 % less PM at a given NO_X level, thus providing additional control flexibility. Ezzitouni et al. [23] tried tuning the pilot fuel injection and found that delaying the pilot fuel improves thermal efficiency, especially under cold-start conditions. Similarly, Mikulski et al. [24] concluded that late pilot injection supported more complete combustion, thus improving combustion efficiency. However, this strategy substantially increased PM emissions, because the main fuel combustion was advanced and thus, less premixed. Liu et al. [25] used double pilot injection and found that for HVO (note that 40 % of DF was admixed to HVO) only combustion of the first pilot fuel was advanced. The remaining doses burnt with similar timings and rates for HVO, DF and also for FAME. Dimitriadis et al. [26] performed parametric study into combustion and emission sensitivities to variable pilot injection and main injection timings. The reported complex trends in emissions and efficiency characteristics resulted from the superposition of effects discussed above.

As split injection strategy calibration proves to be the focus of contemporary engine research related to HVO, full advantages of this fuel can manifest at high EGR rates. While this strategy promises huge NO_X reduction potential, most fuels suitable for CI engines are limited in

terms of their EGR rate by rapidly increasing PM and CO emissions. Due to its high reactivity (high CN) and natural propensity to produce less PM, HVO offers much better trade-offs in this respect. This was confirmed in studies by Liu et al. [25] and Lehto et al. [27]. Importantly, the latter study showed simultaneous reduction of both PM and NO_X by application of the Miller cycle, combined with advanced start of injection (SoI). A follow-up study by Heikkilä et al. [28] demonstrated that this strategy also provides lower particulate number and produces smaller particles.

The study by Lehto et al. [27] revealed an interesting phenomenon, whereby the general trend of increasing PM with EGR was observed to cease at a certain threshold of very high EGR. This indicated a regime shift towards PPCI but was not considered relevant by the authors due to the rapid collapse in efficiency associated with delayed start of combustion. Still, the PM reduction using PPCI mode was far greater for HVO than for DF. HVO's high CN could make it an enabler for efficient low temperature combustion concepts. Driven by this motivation, Hunicz et al. [29] combined an optimised split injection strategy with ultra-high EGR rates, achieving efficient PPCI of HVO with engine-out NO_X and CO emissions near Euro VI limits. Ultimately, efficiency was 1.5 percentage points above the optimised DF baseline. This potential for both superior efficiency and low emissions appeared only in a very narrow spectrum of the calibration map and so far has not been confirmed by other studies.

The results discussed above, highlight the necessity for coordinated air–fuel control when optimising HVO combustion. With this in mind, Omari et al. [30] cross-optimised injection timing, injection pressure and EGR. Across the complete WLTP cycle, the HVO-optimised engine had 65 % lower UHC and CO emissions than the DF-optimised baseline. More importantly, with the same NO_X emissions, PM was almost halved. The conclusions drawn from this endeavour are that HVO works better with high EGR with advanced combustion onsets, while reducing the dwell between pilot and main injections. Additionally, at low loads, fuel injection pressure could be lowered without emission deterioration [31], providing reduction of high-pressure pump parasitic losses, an effect highlighted in recent work by Hunicz et al. [32].

It is evident from the above discussion that engine research into HVO still has more open routes rather than concluded stories. Higher reactivity and narrower range of molecular structure result in different than DF response to combustion control parameters. Even though HVO has been identified as an enabler for efficient and low-emissive PPCI combustion, the investigation of advanced injection/airpath strategies enabled by more sophisticated engine management solutions in prototype engines is still at an early stage. On the air-path side, for example, the co-control of λ and EGR has yet to be evaluated to a sufficient extent. The present study aims to explore this design space while operating an HVO-fuelled engine at the bridge of conventional diesel combustion and PPCI modes. It is vital to fill these knowledge gaps in order to allow transport sectors with a high energy demand to switch to low-carbon fuels and comply with ever-tighter emission limits.

2. Materials and methods

2.1. The fuels

The HVO used for the tests was Neste's commercially available renewable diesel. It is 99 % pure HVO, with a small amount of lubricity improver to meet the requirements of modern diesel injection systems. Commercially available EN 590 DF was the baseline fuel to provide the reference for engine performance and emission results. Neither of the fuels contained any FAME, thus improving the clarity and reliability of the results. Table 1 summarises the fuels physical and chemical parameters relevant to the discussion, and Fig. 1 shows their respective distillation curves.

The parameters for HVO were determined by the VEBIC fuel laboratory, Vaasa, Finland while DF characterisation was courtesy of the Water Transport and Environmental Laboratory of Klaipeda University, Lithuania. Both fuels were analysed using the same methods according to EN 590 and other related standards. Hydrocracking is relatively insensitive to feedstock quality and both test fuels (HVO and DF) used in the study comply with the same standards. Table 1 and Fig. 1 show the major differences in physicochemical properties. These differences were examined in the introduction section, discussing how their combined effects impact on combustion phenomenology. The discussion of the obtained results makes references to specific numerical values presented in this table and the figure.

Table 1
Fuel properties of DF and HVO.

Parameter	DF	HVO
Density @ 15 °C	837 g/l	778 g/l
Kinematic viscosity @ 40 °C	2.94 mm^2/s	2.86 mm^2/s
Lower heating value (LHV)	42.8 MJ/kg	43.9 MJ/kg
Cetane number (CN)	54.1	74.7
Cold filter plugging point (CFPP)	–22 °C	−35 °C
Flash point (FP)	70.5 °C	81.5 °C
Lubricity @ 60 °C	406 µm	344 µm
Carbon to hydrogen ratio (C/H)	6.4:1	5.6:1
Sulphur content	6.1 mg/kg	<1 mg/kg
Ash content	0.014 %wt.	0.002 %wt.

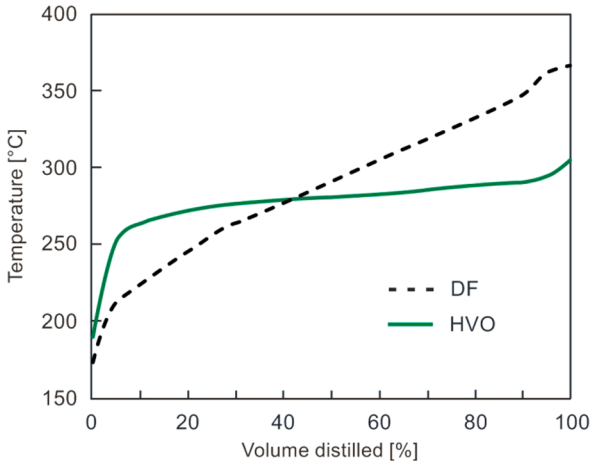

Fig. 1. Distillation curves of DF and HVO.

2.2. The engine tests

2.2.1. Experimental set-up

Detailed engine experiments and related research were performed at the Lublin University of Technology, Poland. The subject of the research was a state-of-the-art, four-stroke, light-duty, single-cylinder AVL 5402 CR DI diesel engine. Table 2 lists its key specifications.

The test engine had a displacement of 510 cm^3 and a compression ratio of 17:1. The piston had a toroidal combustion chamber. The cylinder head was a four-valve design, equipped with tangential and helical ports to control swirl. In the current experiment, both inlet ports were open, resulting in a swirl ratio of 1.7. Fuel was delivered by a seven-hole electromagnetic injector, supplied by a Bosch CP4.1 high-pressure pump. Fuel injection parameters were managed by a fully open engine controller (from Bosch) and Etas INCA software. The fuel delivery system accommodated an AVL 733S dynamic fuel meter and AVL 753C fuel temperature conditioner. Fig. 2 illustrates both the fuelling and the airpath configurations.

The engine was coupled to an externally driven Roots-type Eaton M45 compressor, capable of providing up to 2 bar boost pressure (Figs. 2 – 27). The air path also included a set of filters, a controllable charge air-cooler and a plenum chamber. The EGR system consisted of a butterfly

Table 2
Research engine specifications.

Type	AVL 5402
Configuration	four-stroke, single-cylinder
Bore	85 mm
Stroke	90 mm
Displacement	510.5 cm^3
Compression ratio	17:1
No. of valves	4
Combustion type	Direct injection
Max. fuel injection pressure	180 MPa
Injection system	Common rail, Bosch CP4.1
Engine management	AVL-RPEMS, ETK7-Bosch
Intake valve opening	712 CAD*
Intake valve closing	226 CAD*
Exhaust valve opening	488 CAD*
Exhaust valve closing	18 CAD*
Max. engine load (IMEP#)	2.4 MPa

*CAD – Crank angle degree; #IMEP - indicated mean effective pressure

valve to control EGR flow rate, plus a cooler to control temperature. The exhaust system included a plenum chamber, followed by a back-pressure valve to allow high rates of EGR and mimic the effect of the turbine. The air-path sensing included a thermal mass flow meter (Figs. 2 – 24) and a set of pressure and temperature transducers at various locations of the intake, exhaust and EGR runners.

The concentrations of gaseous components in the exhaust gas were measured with an AVL Fourier transform infrared (FTIR) multi-component analytical system. Particulate concentrations were measured with a Maha MPM-4 analyser. The excess air ratio (λ) was determined with a Bosch LSU 4.2 lambda probe and ETAS LA4 lambda meter with appropriate exhaust gas back-pressure correction [33]. The ratio of the engine intake and exhaust CO_2 concentrations was used to quantify the EGR rate. Inlet gas was sampled from the inlet plenum and analysed with a Hermann-Pierburg HGA 400 gas analyser. Table 3 lists the measurement devices, important from the perspective of the current research scope, together with their respective accuracies.

The piezoelectric pressure transducer (AVL GU22C) was installed directly in the engine head and connected to a charge amplifier, provided the relative in-cylinder pressure signal. This signal was automatically pegged with an absolute pressure reference measured at intake and exhaust ports. The high-speed pressure recording was triggered via an optical encoder, with a constant angular resolution of 0.1 crank angle degree (CAD).

The engine was coupled to an asynchronous motor dynamometer with speed control. The test stand was equipped with a thermal conditioning system that guaranteed constant temperature of coolant- and lubricant, independently of the operating point. The test stand's automation system, based on a programmable logic controller and in-house software, governed all thermal parameters and acquired all low-frequency signals.

2.2.2. Data analysis routines

The measurement system recorded 100 consecutive engine cycles at each steady operating point and their averaged values were taken. AVL Boost software was used to provide accurate pressure data post-processing. The software incorporated gas-flow models, estimation of internal EGR and heat transfer using Hohenberg correlation [34]. The measured in-cylinder pressure was subjected to first-law analysis, which computed apparent HRR. The HRR curves shown in the study refer to the gross values, i.e., they include calculated heat transfer rates. The cumulative HRR was used to calculate mass fraction burnt (MFB), which further yielded combustion timing indicators, like location of 50 % MFB (CA50). Fig. 3 provides interpretation of the HRR traces and definitions of combustion timing parameters.

This study did not consider the enginés mechanical losses, so all performance parameters are indicated specific values. The directly measured molar concentrations of exhaust gas components were converted to indicated specific emissions, taking into account the indicated

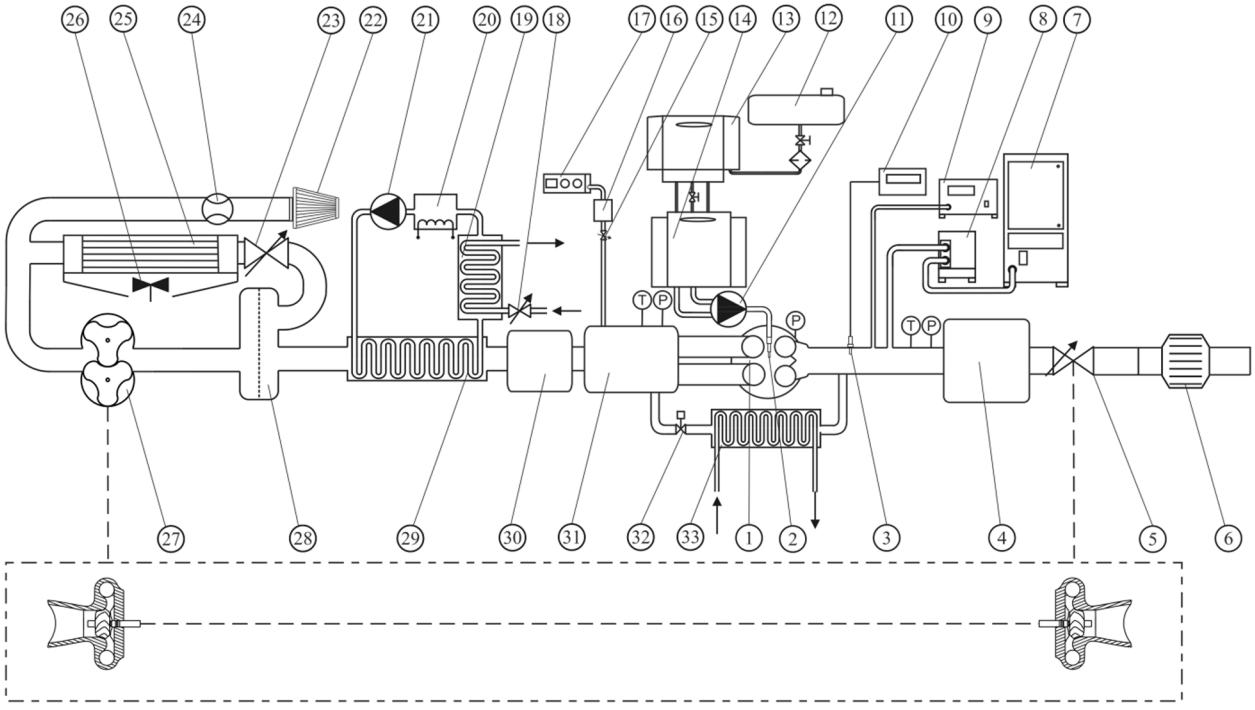

Fig. 2. Schematic diagram of the engine air-path, fuelling and EGR systems: 1 – engine, 2 – fuel injector, 3 – lambda probe, 4 – exhaust plenum, 5 – exhaust back-pressure valve, 6 – exhaust muffler, 7 – FTIR analyser, 8 – heated filter, 9 – MPM-4 PM meter, 10 – lambda meter, 11 – high-pressure fuel pump, 12 – fuel tank, 13 – fuel balance, 14 – fuel conditioner, 15 – pressure control valve, 16 – expansion chamber, 17 – intake gas analyser, 18 – control valve, 19 – air heat exchanger, 20 – air coolant electric heater, 21 – air coolant pump, 22 – air filter, 23 – by-pass valve, 24 – air-flow meter, 25 – air cooler, 26 – air cooler fan, 27 – Roots compressor, 28 – oil separator, 29 - air coolant - air heat exchanger, 30 – intake plenum, 31 – EGR mixing chamber, 32 – EGR control valve, 33 – controllable EGR cooler.

Table 3
Measurement equipment and accuracy.

Measured quantity	Transducer		Meas. range	Accuracy
In-cylinder pressure	AVL GU22C		0–25 MPa	0.25–1.0 %[1)]
Fuel consumption	AVL Fuel Mass Flow Meter 733S		0–125 kg/h	0.12 %
Excess air ratio (λ)	Bosch LSU 4.2 / ETAS LA4		0.7–2.8	1.5 %
Air mass flow rate	Bosch HFM5		8–370 kg/h	3 %
Intake/exhaust press.	WIKA A-10		0–4 bar	0.5 %
Temperatures (ambient, intake air, EGR, cooling, oil, fuel)	Pt100 Czaki TP-361		−40–400 °C	0.2 %
Exhaust temperature	Thermocouple K Czaki TP-204		0–1200 °C	0.8 %
Exhaust composition (gaseous compounds)	AVL Sesam FTIR	CO:	1–10000 ppm	0.36 %
		HC:		0.1–0.49 %[3)]
		NO_X:	1–1000 ppm[2)]	0.31 %
			1–4000 ppm	
PM concentration	Maha MPM4		0–700 mg/m^3	0.1 mg/m^3
Intake composition	Hermann-Pierburg HGA 400	CO_2:	0–20 %	0.1 %
		O_2:	0–22 %	0.01 %

[1)] Depending on temperature.
[2)] Given measurement span relates to concentration of a single identified hydrocarbon.
[3)] Depending on type of hydrocarbon species.

specific fuel consumption (ISFC), the exhaust gas flow rate and density. PM emissions were provided by the measurement device as mass per volume, and then corrected to indicated-specific values.

Either the standard deviation or the device accuracy (Table 3), whichever is higher, were taken as the maximum uncertainty of directly measured parameters. The uncertainty for indirectly calculated parameters was derived from the maximum errors of the directly measured inputs (Table 3). The study performed by Kline and McClintock [35] provides a detailed discussion of the exact differential method used. Note that uncertainties are mentioned specifically in the discussion only when differences in the results between individual fuels are below or close to the level of significance, thus influencing the interpretation. Otherwise, uncertainty is omitted in pursuit of clarity and brevity.

2.2.3. Scope and conditions of the tests

The experiments focused on a single, mid-load operating point. The rotational speed of the engine was fixed at 1,500 rpm and the mass of fuel was 15.2 mg/cycle for DF and 14.8 mg/cycle for HVO. These fuelling rates provide the same energy input of 650 J/cycle and net indicated mean effective pressure (IMEP) around 0.5 MPa (efficiency dependent) for non-EGR operation. The exhaust back-pressure was increased, together with the boost level, to mimic operation of a turbocharger and to enable flow through the high-pressure EGR system. The intake-air conditioning unit maintained a constant air temperature of 25 °C, independent of boost pressure. The temperature of recirculated exhaust gas entering the intake manifold was maintained at a constant level of 85 °C. It should be noted that the aspirated air temperature results from enthalpy balance between fresh air and recirculated exhaust. This temperature was left uncontrolled, replicating normal engine operation. Temperatures of the engine coolant and lubrication oil were set at 85 °C. The fuel-rail pressure was set at 80 MPa to avoid wall-wetting with early injection timings. The fuel temperature before the high-pressure pump was 30 °C for all experiments.

The engine was operated using an HVO-optimised injection strategy, derived from the previous studies of the authors [24,29]. A pilot injection, accounting for 10 % of the total fuel value, commenced at start of injection for pilot injection (SoI_p) = 18 CAD before top dead centre (TDC). The main dose of fuel was injected at start of injection for main injection (SoI_m) = 6 CAD before TDC. The injector rig tests have shown that at such injection parameters and 1500 rpm, physical fuel flow finished in less than a single CAD after tuning off the excitation signal reference [36]. As the min injection was completed before the start of the high-temperature heat release (see Fig. 3), such a strategy resulted in PPCI combustion, while maximising thermal efficiency by phasing the combustion near TDC. Various tests at different dwells between sequential injections and at different pilot injection fuel mass fractions shown that the selected injection strategy provided the best NO_X-PM trade-off at wide EGR conditions for naturally aspirated operation [29].

This study's experimental matrix entailed parameter sweeps of intake manifold absolute pressure (MAP), from atmospheric to moderate boost (MAP ≈ 165 kPa), with variable EGR valve positions, providing different configurations of diluents composition. Fig. 4a depicts the span of achieved EGR rates and λ values. Fig. 4b reveals the detail of an exemplary constant lambda (λ = 2) sweep, in terms of MAP and EGR rates. Similarly, Fig. 4c shows how MAP determines λ value, at non-EGR conditions.

At each point of Fig. 4, the engine was thermally stabilised and all governing parameters, except those controlled in a closed-loop (temperatures of all media, engine dynamometer speed control and Roots compressor speed) were fixed. After stabilisation, in-cylinder pressure data were recorded for 100 consecutive cycles. It should be noted that the coefficient of variation in IMEP did not exceed 2% at any operating point. At stabilised conditions, all slow-changing parameters (e.g., flows, pressures, temperatures and data from gas analysers) were sampled every 1 s and time-averaged within a 60-second measurement window.

3. Results and discussion

3.1. Combustion analysis – Selected sweeps

Figs. 5 to 7 show gross HRR and MFB curves for different mixture compositions. They demonstrate that, at the given injection strategy, neither EGR, λ nor MAP affects main fuel combustion to a large extent. For both DF and HVO, the fast-progressing, high-temperature heat release of the main fuel dose starts at TDC. This accommodates both the premixed phase and the diffusion-controlled combustion within the developing spray. The transition moment, when premixed combustion ends, is distinguishable for both DF and HVO as an inflection point on the main HRR curve. The location of this transition point, however, depends on the fuel and mixture conditions.

The insensitivity of the main combustion to air-path parameters stems from the fact that the event is controlled by the already-developed flame of the pilot. More specifically, the main fuel dose ignites when the

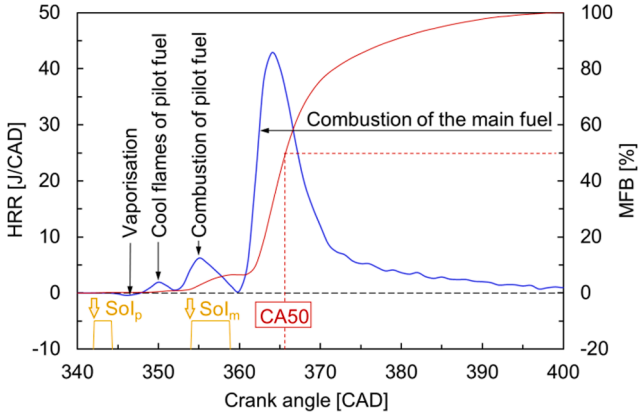

Fig. 3. Example of HRR and MFB curves, with their interpretation and definitions of the combustion timing data.

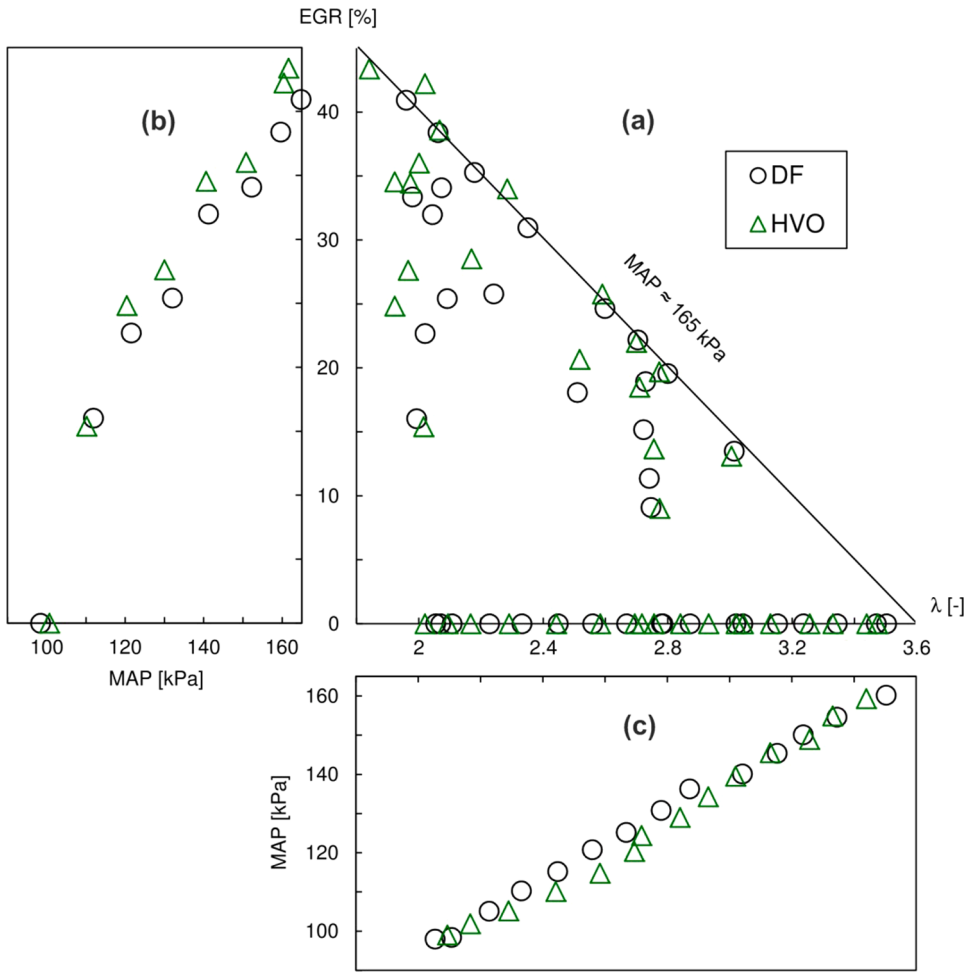

Fig. 4. EGR and λ map for all investigated conditions (a), MAP required to achieve the investigated EGR span at λ ≈ 2 (b) and MAP required to achieve investigated λ range at non-EGR conditions (c).

spray front reaches the hot region of pilot-combustion products. This pilot combustion, initiating around 346–347 CAD, is much more sensitive to fuel dilution than is the main combustion. Increasing fuel dilution by either EGR or greater fresh air aspiration (MAP) advances pilot combustion and increases the amount of fuel consumed in this stage. More details on the fuel-to-fuel differences and diluent effects are provided below.

3.1.1. *Effect of excess air*

Fig. 5 shows the HRR curves of selected points of the λ sweep performed without external EGR (Fig. 4c). The pilot combustion accommodates the initial low-temperature phase (so-called cool-flames and negative temperature coefficient reactions) and the following high-temperature, premixed-in-nature combustion of the developed pilot spray. The separation between the two phases is visible in Fig. 5 for both DF and HVO at λ = 2.05–2.08. The transition point is less evident at leaner mixtures because high-temperature combustion commences earlier, taking advantage of higher oxidiser entrainment rates. Higher oxidiser availability reduces the chemical ignition delay controlling the high-temperature phase of the pilot fuel.

At this point, there is evidence of the difference in the two fuels' CN values, resulting from both - physical and chemical properties. Firstly, HVO contains hydrogenated long-chain hydrocarbons of well-defined composition (majorly near C_{10} to C_{12}), while DF is a mixture of several different hydrocarbons ranging from C_8 to C_{18} [37]. This results in a much lower distillation temperature of HVO (see Fig. 1 for reference) and its reduced viscosity (Table 1), supporting faster vaporisation than in the case of DF. Secondly, more reactive paraffinic fuel has significantly shorter chemical ignition delay. As a result, the pilot combustion is both earlier and more rapid compared to DF (compare the early-stage HRRs between Fig. 5a and b).

Detail analysis of the cumulative heat release during pilot fuel combustion, shown in Fig. 6, reveals interesting observations relating to λ and fuel. For DF, the MFB at the start of main fuel combustion varies from 8 % of the total fuel at λ = 2.05, to 9 % at λ = 3.23. For HVO, a noticeably larger amount of energy is released during the early premixed phase, totalling 9 % to 11 % for the corresponding λ range. HVO thus exhibits a higher degree of complete combustion for pilot injection. This is attributable to its higher CN and lower viscosity giving better fuel atomisation, and it leaves less fuel transferred to the main combustion phase. It should be noted that the pilot fuel was burnt completely during the first combustion stage for HVO at λ = 3.25.

While the main injection commences, it is interesting to note the quenching effect of the main fuel vaporisation on the pilot combustion. This effect is visible both in Fig. 5 and Fig. 6 and is most pronounced for DF at richer mixtures. It can be noticed in Fig. 5a that the main fuel injection overlaps the first stage of combustion (pilot combustion). This further hinders the early-pilot heat release, translating to elongated (hence less efficient) main combustion. Either applying boost (supplying more oxidiser) or using a more reactive fuel like HVO compensates for this deficit of the considered injection strategy. In the case of HVO, the pilot combustion is almost completed before SoI_m. More heat released in the initial combustion stage translates into a slightly earlier start of the main combustion. This explains the combustion response to both boost

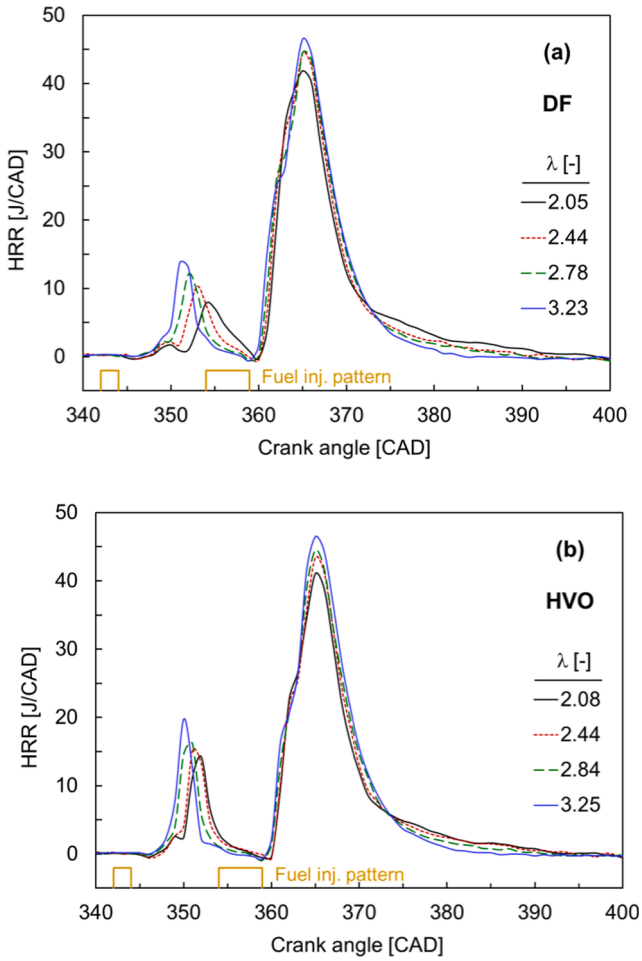

Fig. 5. HRR curves for λ sweeps at non-EGR conditions. DF and HVO are analysed at similar conditions.

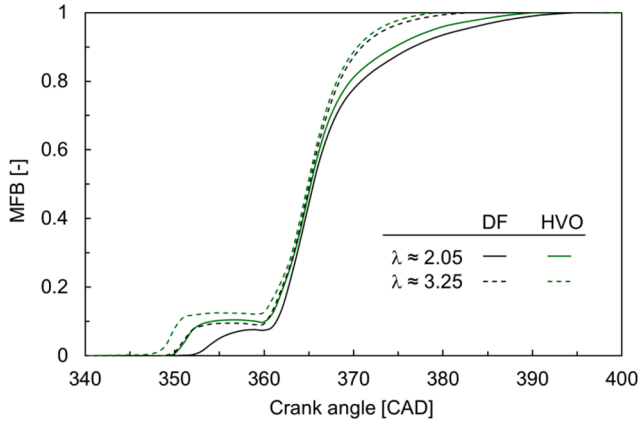

Fig. 6. MFB curves for both fuels at different λ. Non-EGR conditions.

and fuel reactivity. It should be noted that the start of main fuel combustion (local minimum on the HRR curve in Fig. 5) was shifted by a single CAD for both fuels for a given range of λ.

Referring back to Fig. 5, the inflexion points on the main heat release (approximately at 362–363 CAD) deserve additional comment. These points indicate the transition from premixed to diffusion-controlled combustion related to the main injection. For both test fuels, the advancement in the main combustion resulted in earlier switching of the modes. This is plausible because the mixing time is reduced.

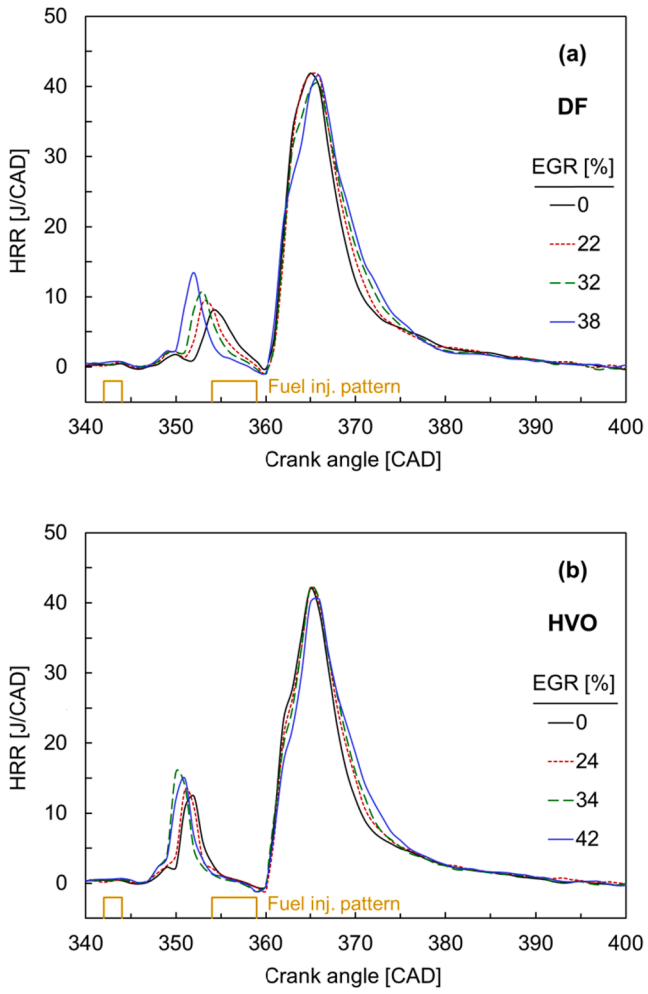

Fig. 7. HRR curves for EGR sweeps and constant λ ≈ 2. DF and HVO are analysed at similar conditions.

Interestingly, independently of the first stage of combustion, the main combustion regime switch appears at approximately 20 % MFB, and this is also independent of fuel. It is also worth noting that the afterburning stage, which starts at approximately 375 CAD, is strongly affected by the mixture strength. Namely, for lean mixtures, the last stage of combustion runs at a lower HRR.

3.1.2. *Effect of EGR*

Fig. 7 depicts the HRR curves for different EGR rates. Note that the intake temperature is determined by the enthalpy balance between the fresh air (conditioned at 25 °C) and recirculated exhaust gas, independently conditioned at 85 °C. Thus, increasing the EGR rate also increases the intake temperature, from 25 °C (at 0 % EGR) to approximately 60 °C (at 39 % EGR). With the higher heat capacity of EGR, however, the differences in intake valve closing temperatures are almost completely compensated during the compression.

The MAP range in the EGR sweep in Fig. 7 is similar to that of the λ sweep (section 3.1.1), ranging from 100 kPa to approximately 165 kPa. Qualitatively, the effects on combustion are also observed to be similar, regardless of whether the fuel dilution is achieved by air (as in Fig. 5) or EGR (Fig. 7). Increasing the EGR rate for the fixed λ advances the high-temperature combustion phase of the pilot fuel. Additionally, the high-temperature heat release from the pilot DF combustion is quenched by the main injection, similar to the behaviour apparent in Fig. 5a. However, the start of main combustion is completely unaffected by EGR, as shown in Fig. 7. This observation proves that there is a balance between

the heat released in the pilot stage, the intake temperature and the specific heat (resulting from EGR) in this sweep: this balance leaves the start of main combustion unaffected. There is also a slight difference in the location of inflection points on the main HRR curves, showing that increasing the EGR rate advances the transition from premixed to mixing-controlled combustion. An interesting difference between the λ sweep (Fig. 5) and EGR sweep (Fig. 7) is that the HRR curves for all the EGR values follow each other very closely indeed during the afterburning combustion phase, starting from approximately 375 CAD. This suggests that the late combustion phase is controlled solely by the excess air.

While the main combustion remains insensitive to EGR for both DF and HVO (due to the mentioned balancing effect in the mixturés thermal state), the fuel-to-fuel differences manifest in the pilot combustion stage, with possible impact on emission formation. For DF, the EGR has an accelerating effect on the pilot combustion, gradually increasing the peak HRR. The autoignition-supporting effect of increasing intake temperature dominates the oxygen deficit introduced by EGR. HVO, on the other hand, exhibits far less sensitivity to EGR in terms of the early pilot combustion – an effect attributed to the high CN of the fuel.

3.1.3. Summarising the performance indicators

The observations from HRR analysis in sections 3.1.1 and 3.1.2 are brought together in Fig. 8, which shows CA50 for the λ sweep and the EGR sweeps, the latter performed both at constant λ ≈ 2 and at constant MAP ≈ 165 kPa. Increasing the MAP, and consequently λ, at non-EGR conditions advanced the CA50 by less than a single CAD for both test fuels, as shown in Fig. 8a. Ultimately, this advance is approximately 0.2 CAD larger for HVO compared to DF for the investigated range.

The effect of λ on CA50 is also present when analysing the EGR sweep at constant MAP (solid lines in Fig. 8b). In this case, the effect of fuel seemed similar to that described in the previous paragraph, whereas the mixture composition effect combines λ and EGR. Increasing the EGR reduces the λ value but also simultaneously reduces the overall specific heat. This explains why the increase in CA50 in Fig. 8b is larger than would occur if reducing only λ, as in Fig. 8a. It should be noted that non-EGR conditions at MAP ≈ 165 kPa in Fig. 8b overlap the maximum λ points in Fig. 8a.

The effect of EGR at constant λ (dashed lines in Fig. 8b) is less evident than its effect at constant MAP. Careful analysis of Figs. 5 and 7 provides support to explain this difference. For both the "clean" lambda sweep (Fig. 5) and the EGR sweep (Fig. 7), the earlier pilot fuel combustion is compensated by the longer main combustion stage. However, increasing the EGR fraction does not affect the afterburning period. Thus, in the case of the sweep varying λ without EGR, the amount of heat released during the afterburning period is the sole factor that determines variations in CA50.

As a final note regarding combustion phasing, it should be stated that split injection eliminates the differences between fuels and mixture compositions in terms of the main fuel combustion rate – hence the overall minor changes in CA50 observed in Fig. 8. These minor changes are driven solely by the pilot fuel combustion, which affects the main fuel ignition delay. The larger amount of heat released from the pilot in the initial combustion stage correlates to the earlier start of main combustion. This observation helps understanding of the combustion control mechanisms in a split-injection strategy, regardless of fuel, EGR or λ.

Turning to the effect of fuel on engine performance, maximum efficiency is achieved when CA50 is orientated close to TDC. Comparison of Figs. 8 and 9 shows a close correlation between CA50 and indicated thermal efficiency (ITE). This correlation shows that high excess air (high boost) and non-EGR conditions support the efficient transition of combustion energy to useful cylinder work. However, the fuelś ability to maintain favourable combustion timing has a secondary effect on ITE.

The primary reason for the trends observed in Fig. 9 is related to mixture composition with: (i) increased EGR reducing the adiabatic exponent, which impacts thermodynamic cycle efficiency, (ii) increase of boost reducing overall temperature and thus heat transfer losses. Thus, increasing EGR at constant MAP had a far greater effect on ITE (solid line in Fig. 9b) than the EGR sweep performed at constant λ (dashed line in Fig. 9b). In the first scenario, the amount of in-cylinder charge is approximately constant: the increased amount of EGR reduced the amount of fresh air aspired, so effects (i) and (ii) act together with retarded CA50 to penalise efficiency. ITE drops by 1.5 and 2 percentage points for DF and HVO respectively when moving from the non-EGR case to 42 % EGR along the constant MAP line. In contrast, for a constant λ scenario (dashed lines in Fig. 9b), EGŔs deleterious effect on efficiency is compensated by an equal increase in aspirated air.

The same general trends in ITE are observed for both fuels, but HVO combustion provides on average 0.4 percentage point better efficiency than DF. This advantage can be marginally justified by the earlier CA50 exhibited by HVO, but primarily it stems from HVO's propensity to achieve higher degree of complete combustion, with fuel-to-fuel

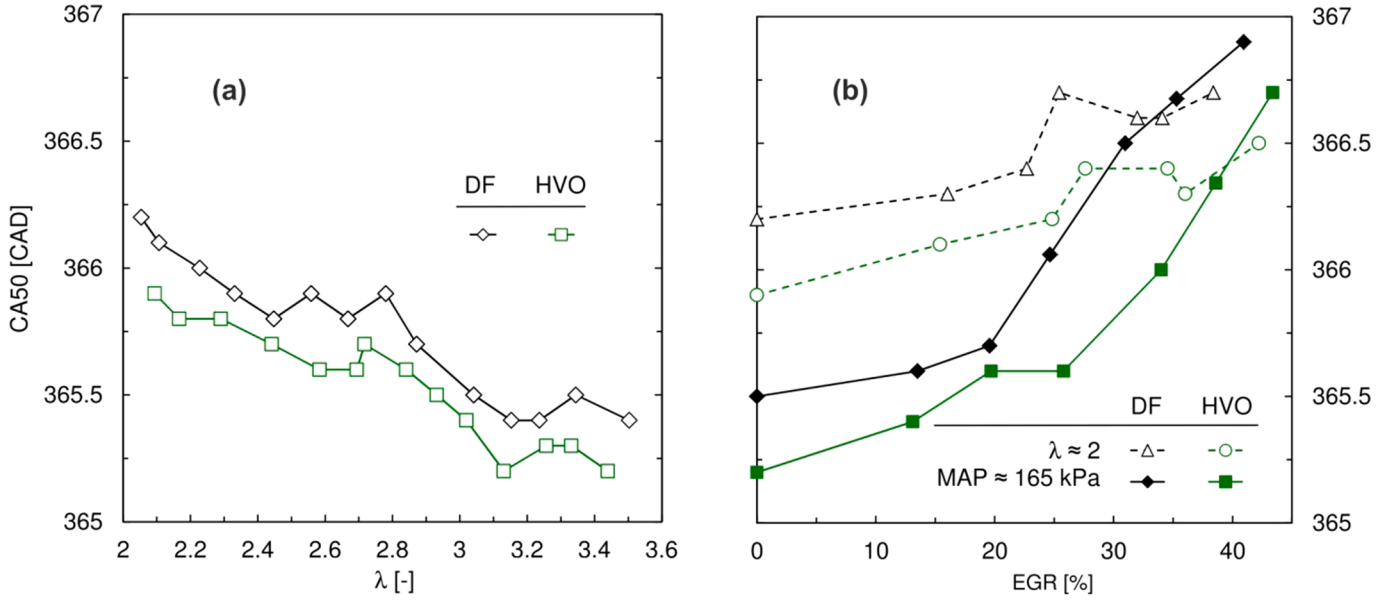

Fig. 8. Locations of 50% MFB; (a) λ sweep at non-EGR conditions, (b) EGR sweeps at constant λ and constant MAP.

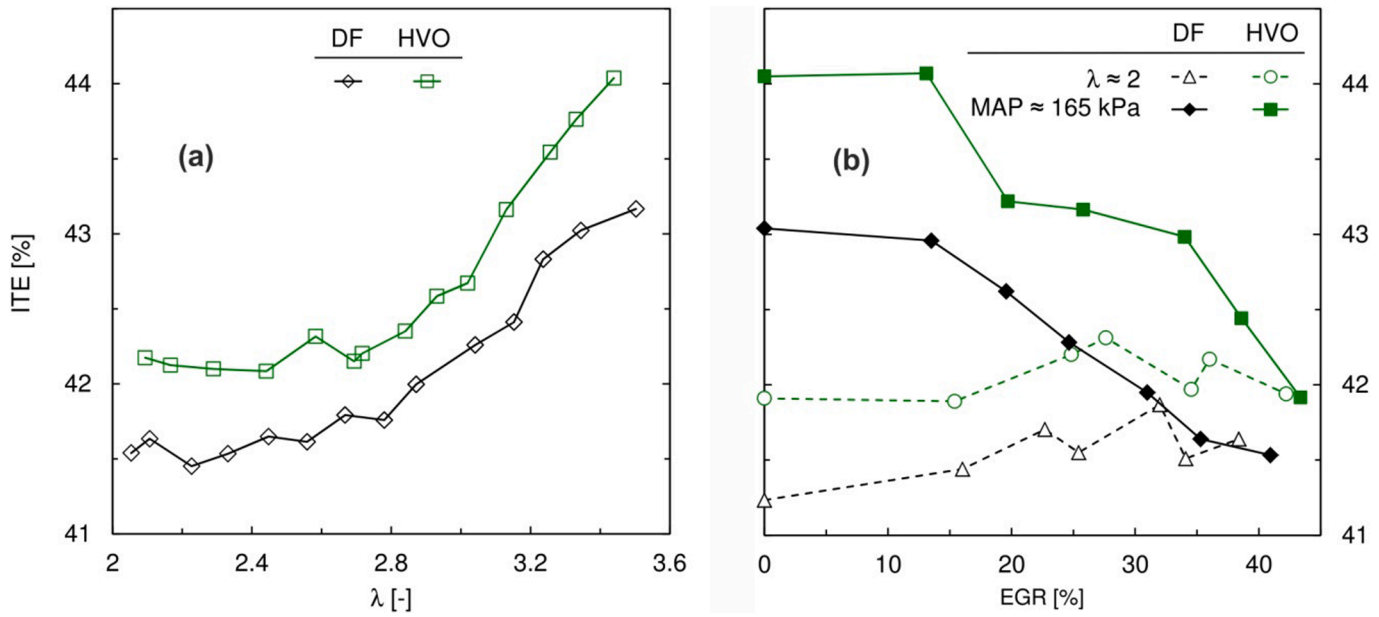

Fig. 9. Indicated thermal efficiency; (a) λ sweep at non-EGR conditions, (b) EGR sweeps at constant λ and constant MAP. The maximum uncertainty of ITE is ± 0.2 percentage points.

differences in combustion efficiency ranging from 0.1 to 0.2 percentage points. Section 3.3 includes a discussion of the general effects of individual air-path management strategies on both fuels. It should be noted that the efficiency differences between HVO and DF, although consistent and phenomenologically justified, are barely above the level of statistical significance, with a maximum uncertainty in ITE at ± 0.2 percentage points.

3.2. Emission analysis

The previous section concluded that the sweeps of λ and EGR did not have a pronounced effect on the onset of combustion at the provided injection strategy. This statement holds true for both the reference DF and HVO. Despite this insensitivity in terms of overall combustion timing, the changes in the premixed, pilot combustion phase and differences in global and local mixture conditions are significant and important. They translate into major differences in PM and NO_X emissions between the fuels when sweeping the λ or EGR.

3.2.1. PM emissions

Fig. 10 shows PM emissions for the λ sweep at non-EGR conditions and both EGR sweeps discussed in section 3.1.3. It is clearly evident that HVO produces significantly lower PM emissions than the reference DF. This advantage results from HVO's narrow hydrocarbon range and low distillation temperature. This feature supports generating a more homogeneous mixture that is less prone to soot formation. Furthermore, HVO contains almost no sulphur or aromatics which are chemical precursors of soot formation.

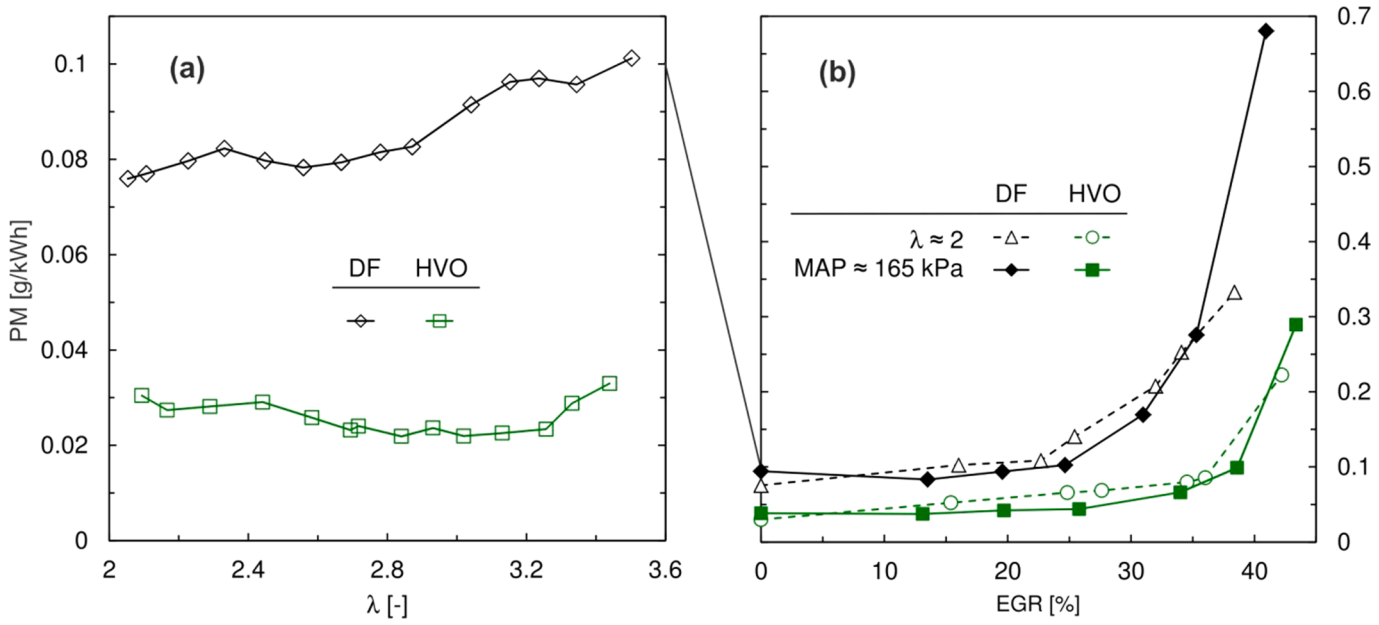

Fig. 10. Indicated specific PM emissions; (a) λ sweep at non-EGR conditions, (b) EGR sweeps at constant λ and constant MAP. Note different scales of *y*-axes in Figs. a and b.

Fig. 10a also shows that HVÓs PM emissions are not sensitive to changes in lambda in the wide range of applicable boost pressures for the non-EGR case. It should be noted that this trend is broken by approaching the upper limit in boost pressure: HVÓs PM emissions start to rise with increasing λ value above 3.2. DF, on the other hand, exhibits a steady linear trend in PM emissions, where increasing λ from 2 to 3.5 elevates the PM emission by approximately 15 %. In general, the increase in PM with increasing λ can be attributed to the in-cylinder fluid density effect on fuel spray penetration. Higher boost pressures produce correspondingly higher in-cylinder fluid density during the injection phase, suppressing the spray penetration. With a less-premixed mixture, the reduced local oxygen availability is the dominating mechanism responsible for increased PM emissions at higher boost pressure, despite the increased excess air.

The different sensitivities of the tested fuels to mixture composition become pronounced when EGR is taken into consideration, as shown in Fig. 10b. In addition to generally lower PM emission, HVO shows another advantage which manifests as lower sensitivity to EGR. Namely, PM emission with DF increases rapidly for EGR levels above 25 %, doubling when EGR changes from 25 % to 33 %. However, for HVO, this inflection point appears later, occurring when EGR rates rise above 35 %. For DF, the PM threshold of 0.1 g/kWh emission is exceeded when EGR varies from 15 % to 25 %, depending on boost and the resultant λ value. Within this same PM emission threshold, HVO accepts EGR rates at least 10 percentage points higher. Alternatively speaking, HVO accepts 35 % EGR while still generating lower PM emissions than the DF non-EGR reference.

Clearly, HVÓs high CN provides the advantages of a higher degree of complete combustion and smokeless combustion under heavy EGR conditions. In this regime, less-reactive DF exhibited issues with ignitability at the early premixed phase, which is responsible for the rapid PM emission increase. This is despite the similarities between DF́s and HVÓs diffusion-based combustion characteristics.

Comparison of the EGR sweeps in Fig. 10b shows that the constant MAP strategy provides lower PM emission than the constant λ approach for moderate EGR rates (between 10 % and 35 %). For DF, the PM results changed in favour of the $\lambda = 2$ trend line only after the EGR rate exceeded 35 %. This relates directly to the global oxidiser availability, which supresses PM formation. The 35 % EGR point with MAP at 165 kPa corresponds to the λ value of approximately 2, so emissions are observed to be similar for both sweeps at this point. EGR rates below 35 % with the same MAP are points with $\lambda > 2$

A peculiar effect can be observed in the low-EGR regime for the constant MAP trend in Fig. 10b. Starting from the non-EGR point, the first increase of the recirculation rate reduces PM emission for both test fuels. This can be attributed to the combined effects of λ and EGR. Namely, it was already observed in Fig. 10a that raising λ above 3 slightly increased the PM emission. Thus, PM emission decreases because the PM formation effect of EGR is dominated by decreasing λ. Additionally, the increase in EGR at constant MAP reduced the amounts of exhaust gas, reducing calculated emissions at a given component concentration.

3.2.2. NO_X emissions

For both fuels at non-EGR conditions, elevating λ from 2 to 3.5 generally increases NO_X emissions by 40 % (Fig. 11a). The fuel-to-fuel comparison shows that HVO produces slightly higher NO_X, attributable to its earlier combustion.

The trends shown in Fig. 11b demonstrate the NO_X emission sensitivity to EGR. The addition of EGR reduces the combustion temperature at the given excess air and reduces oxygen availability for the given temperature. Both these approaches drastically reduce NO_X formation. For $\lambda \approx 2$, increasing the EGR rate from 0 to approximately 40 % effectively reduces NO_X from 4.7 g/kWh to around 0.5 g/kWh. Within the level of significance, EGŔs effect on NO_X is the same for DF and HVO.

The EGR sweep at constant MAP ≈ 165 kPa, shown in Fig. 11b, demonstrates an even greater NO_X reduction. This is because its non-EGR baseline carries an emission penalty associated with increased λ. Raising the EGR rate reduces the excess air: when the rate reaches approximately 35 % both fuels have the same NO_X levels as the $\lambda \approx 2$ strategy. An even larger NO_X reduction is observed at constant MAP when the EGR rate exceeds 35 %, but this scenario is comprised by a drastic increase in PM emission, as shown in section 3.2.1.

3.2.3. PM-NO_X trade-off

The general picture emerging from the analysis of individual sweeps is that the PM-NO_X trade-off when using HVO is significantly better than DF́s. The explanation comes from the detailed combustion analysis in section 3.1 and relates to the combined effect of HVÓs higher volatility and higher CN. Fig. 12 distils the trade-off data for all investigated air-

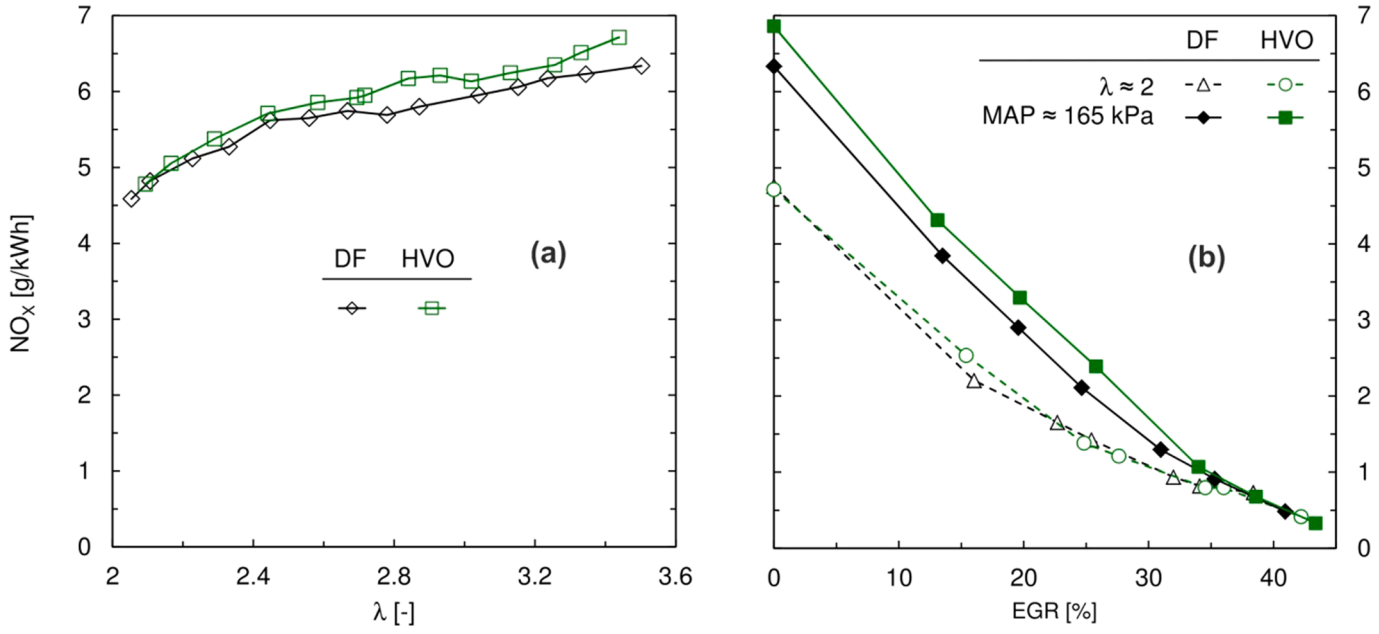

Fig. 11. Indicated specific NO_X emissions; (a) λ sweep at non-EGR conditions, (b) EGR sweeps at constant λ and constant MAP.

path parameters.

For both HVO and DF, the EGR-driven NO_X reduction is accompanied by the penalty of increased PM emissions. However, HVO has the advantage of lower baseline PM emissions at non-EGR conditions (on the right-hand side of Fig. 12). The non-EGR emissions of PM for HVO and DF are 0.03 g/kWh and 0.075 g/kWh respectively. Consequently, HVO offers PM at the level of DF's non-EGR baseline, but simultaneously reducing NO_X to 1 g/kWh via EGR. More importantly, further NO_X reduction to 0.7 g/kWh is possible without exceeding a 0.1 g/kWh PM emission limit. DF cannot match this performance due to a rapid increase in PM production at high EGR rates. Alternatively, reduction of DF́s PM emissions below 0.1 g/kWh is compromised by NO_X emissions of at least 2.5 g/kWh.

Looking at the right-hand side of Fig. 12, it is worth noting that NO_X emissions above 4.3 g/kWh occur only at non-EGR conditions, where the numbers further increase with increased boost. Fig. 12 also shows that PM emissions in this range are hardly affected, so one can conclude that at non-EGR conditions operating at λ above 2 brings no benefits for either fuel. Note that HVO's PM emissions, oscillating around 0.02–0.03 g/kWh, can be considered ultra-low, comparable with those demonstrated in highly premixed, low-temperature combustion concepts [38,39].

3.3. HVO air-path optimised results

To explore the calibrations for an air-path optimised for HVO, within the constraints of other arbitrarily selected control parameters, a so-called over-limit function [40] is proposed. It quantifies both emission factors, NO_X and PM, cumulatively, with respect to their limits, using the following equation:

$$F = \max\left(0, \frac{PM}{PM^*} - 1\right) + \max\left(0, \frac{NO_X}{NO_X^*} - 1\right) \quad (1)$$

The numerators refer to measured emissions and the denominators (*) are the respective heavy-duty Euro VI limits; 0.4 g/kWh for NO_X and 0.01 g/kWh for PM. Efficiency and other emissions are not included in the over-limit function definition because they exhibit far less sensitivity to the air-path calibration than NO_X and PM. Therefore, these parameters would not affect the final result significantly if optimisation is considered.

This synthesis, incorporated into the framework of Fig. 13, clearly shows the air-path preferences of both HVO and DF.

Applying the optimised over-limit function, HVO scores a value of around 6 points, out-performing DF by roughly 100 % . HVÓs best overall emission results are achieved for low lambda of 2.1 and at approximately 25 % EGR. At such conditions, PM and NO_X are at 0.055 g/kWh and 1.4 g/kWh respectively. Fig. 12 shows where the optimised conditions for HVO and DF occur on the PM-NO_X trade-off fronts. Turning to DF, Fig. 13 shows the best overall emission results are at maximum investigated boost, providing lean mixture (λ = 2.7) at 22 % EGR. This corresponds to 0.08 g/kWh PM and 2.6 g/kWh NO_X. Fig. 14 plots both fueĺs optimised air-path calibrations, together with their results in terms of NO_X, PM, other regulated and unregulated emissions and also fuel efficiency. This effectively summarises the discussion on air-path conditions that provide the lowest emissions.

At higher EGR and lower λ, HVO requires less boost, yielding lower specific heats ratio for the mixture. Nevertheless, ITE is observed to be 1.5 percentage points higher for HVO than for DF. The maximum error in ITE is ± 0.2 percentage point, taking account of the accuracy of fuel consumption measurement and the adopted resolution of pressure trace integration. This statistically significant improvement in ITE translates

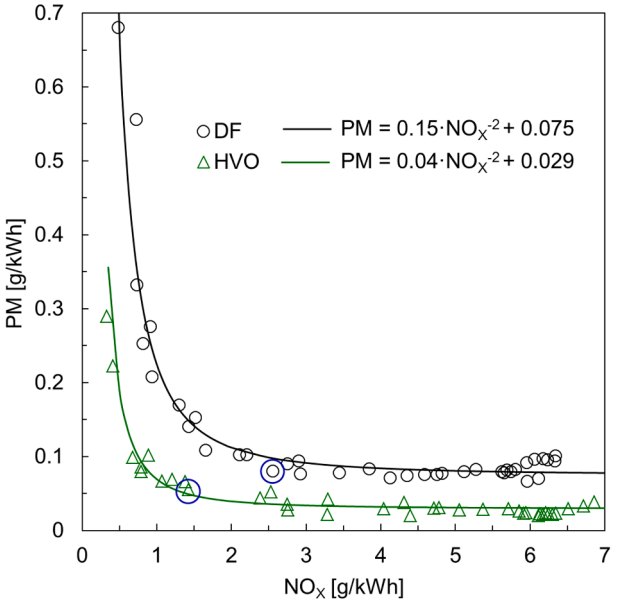

Fig. 12. PM-NO_X trade-off for all investigated conditions. The points selected by blue circles are the ones with the smallest over-limit emission (see section 3.3. for details). (For interpretation of the references to colour in this figure legend, the reader is referred to the web version of this article.)

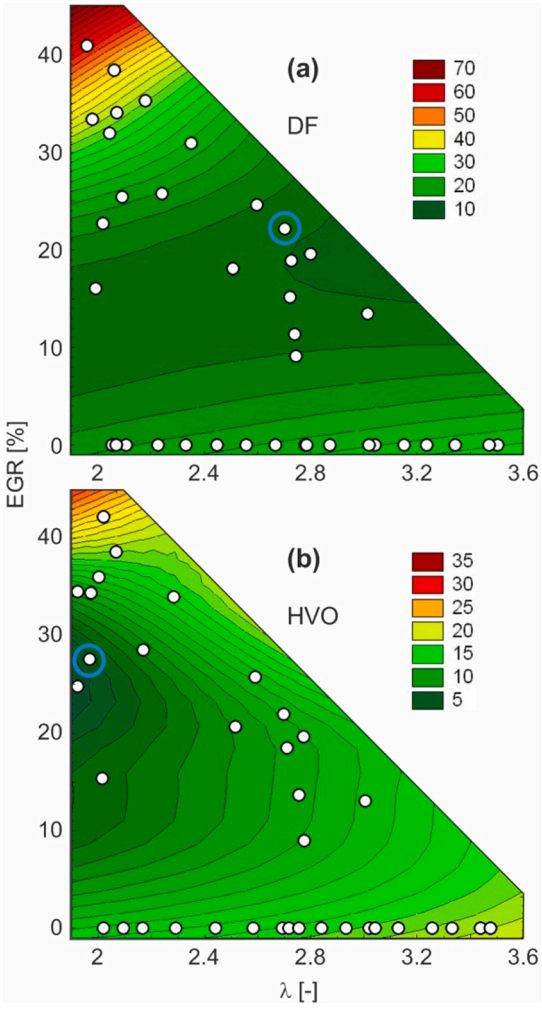

Fig. 13. Maps of the over-limit function values for all investigated conditions. Note different scales. The points marked with blue circles are the ones measured with the smallest emission over-limit. (For interpretation of the references to colour in this figure legend, the reader is referred to the web version of this article.)

into 8 % lower specific CO_2 emission (measured in the exhaust gas), which is equally affected by higher H/C ratio of the fuel (refer to Table 1) and higher efficiency. Both fuels have similar CO levels.

HVO's total hydrocarbon (THC) emissions are 37 % lower than DF́s. Analysis of the non-regulated emissions concluded that octane (C_8H_{18}) accounted for over 50 % of THC from both fuels (Fig. 14). Lower THC emission when the engine is fuelled with HVO is primarily attributed to its lower concentration of the principal hydrocarbon, octane. HVO seems to achieve a higher degree of complete combustion, affirmed by a corresponding reduction in short hydrocarbon concentrations, including ethylene (C_2H_4). HVÓs more complete combustion is attributable to higher volatility and lower viscosity. Furthermore, aromatics (AHC) are simply not present in HVO's chemical make-up, and this absence of aromatic emission also contributes to its low THC count. Aromatics are potentially carcinogenic, so this is another advantage for HVO as a cleaner DF substitute.

Note that the above discussed unregulated species results are close to (yet slightly above) the level of statistical insignificance when indicated specific values are considered. This is due to large influence of inaccuracies in fuel consumption measurement and indicated power calculation. It may be noted that the mentioned differences between the two fuelś emissions were consistently observed on the directly measured ppm basis for all operating points. As such, they are not the products of measurement noise. On the other hand, assuming the same definition of significance, HVO and DF both produce similar amounts of formaldehyde, formic acid and acetaldehyde (not shown in Fig. 14).

4. Conclusions

This study explored HVÓs potential for cleaner combustion by means of dedicated EGR and boost strategies. The engine was operated with a split fuel injection strategy, providing partially premixed combustion. The results yield the following conclusions:

- Effects of the λ and EGR on the overall combustion onset are not pronounced, for both HVO and reference DF. Despite this insensitivity, the small changes in the premixed, pilot combustion phase and the resultant impact on local mixture conditions translate into large-scale differences in emissions.
- Optimisation focus for HVO can be narrowed down to PM and NO_X. All other exhaust components and efficiency are far less sensitive to air-path parameter changes.
- NO_X emissions change linearly with EGR, whereas the increase of PM formation is highly progressive. HVO benefits from lower chemical propensity to produce PM, providing more scope for NO_X optimisation.
- An air path optimised for HVO combustion instead of diesel favours higher EGR ratios (25 % vs 20 %) and lower boost pressures (130 kPa vs 165 kPa). At such conditions (λ of 2.1 vs 2.7) overall emissions from HVO were roughly 50 % lower than with optimised DF combustion.
- HVO gives 1.5 percentage points higher indicated efficiency (43.5 %); produces 1.4 g/kWh NO_X (46 % better than best diesel); ultra-low particulates of 0.055 g/kWh (33 % improvement); and 0.3 g/kWh unburnt hydrocarbons (37 % better).
- HVÓs CO emission is roughly the same as DF́s (0.66 g/kWh). Complete elimination of carcinogenic aromatic emissions and 8 % lower tank-to-wheel CO_2 footprint are additional incentives for HVO.

The improvement levels demonstrated in this study are comparable to those obtained in the authorś earlier work to optimise multi-pulse injection parameters [29]. The optimised points in both studies do not overlap, suggesting there is further improvement potential for HVO with coordinated air- and fuel-path control strategies. This multi-objective co-optimisation of HVO combustion, exploring the boundaries of conventional and partially premixed combustion at high EGR rates, will be investigated in a follow-up study.

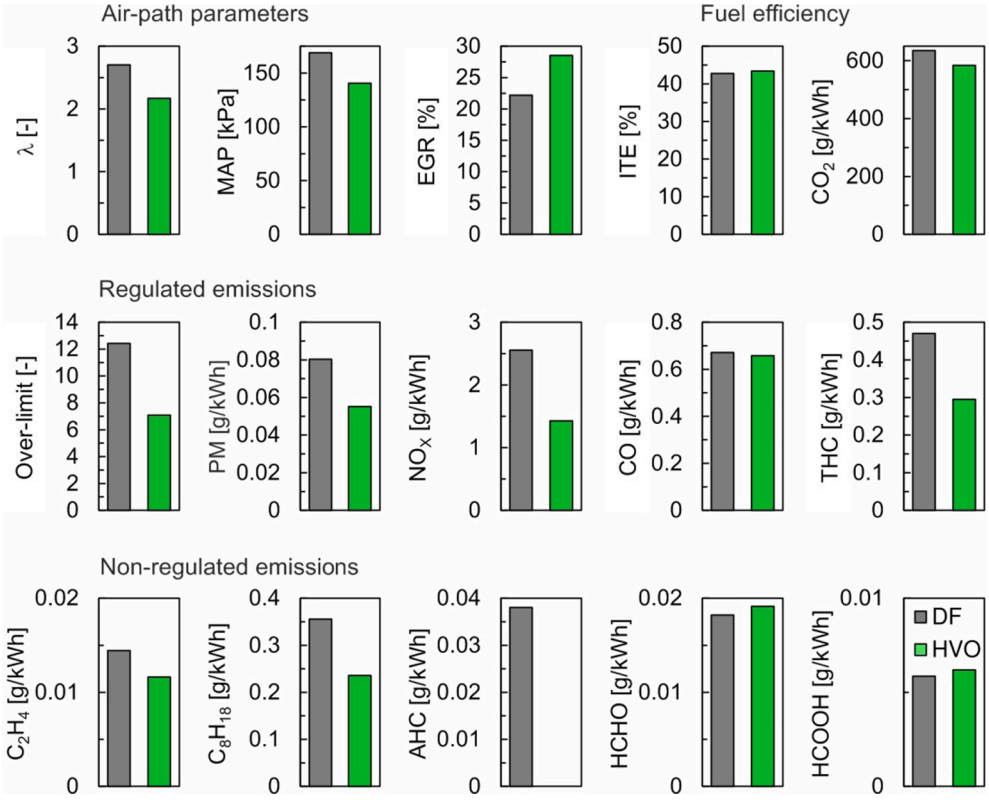

Fig. 14. Fuel-to-fuel comparison at optimal air-path settings; efficiency, regulated emissions and selected non-regulated emissions.

CRediT authorship contribution statement

Jacek Hunicz: Conceptualization, Methodology, Investigation, Formal analysis, Visualization, Writing – original draft, Writing - review & editing, Funding acquisition, Project administration, Supervision. **Maciej Mikulski:** Conceptualization, Investigation, Validation, Resources, Writing – original draft, Writing - review & editing, Funding acquisition, Supervision. **Pravesh Chandra Shukla:** Validation, Writing – original draft, Writing - review & editing. **Michał S. Gęca:** Data curation, Resources, Software.

Declaration of Competing Interest

The authors declare that they have no known competing financial interests or personal relationships that could have appeared to influence the work reported in this paper.

Acknowledgment

The research was financed in the framework of the project Lublin University of Technology, Regional Excellence Initiative, funded by the Polish Ministry of Science and Higher Education (contract No. 030/RID/2018/19).

The authors wish to thank AVL List GmbH for making the simulation software available within a framework of the AVL University Partnership Program.

References

[1] International EPT. https://www.ukimediaevents.com/publication/c141a6ab/1. March 2021:60-1.
[2] Nouvelles IE. https://www.ifpenergiesnouvelles.com/article/biofuels-dashboard-2019; 2021. Available from: https://www.ifpenergiesnouvelles.com/article/biofuels-dashboard-2019. Accessed 16.04.2021.
[3] Liaquat AM, Masjuki HH, Kalam MA, Rizwanul Fattah IM. Impact of biodiesel blend on injector deposit formation. Energy 2014;72:813–23.
[4] Velmurugan K, Sathiyagnanam AP. Effect of biodiesel fuel properties and formation of NO x emissions: a review. Int J Ambient Energy 2017;38(6):644–51.
[5] GRZELAK P, ŻÓŁTOWSKI A. Environmental assessment of the exploitation of diesel engines powered by biofuels. Combustion Engines 2020;180(1):31–5.
[6] No S-Y. Application of hydrotreated vegetable oil from triglyceride based biomass to CI engines - A review. Fuel 2014;115:88–96. https://doi.org/10.1016/j.fuel.2013.07.001.
[7] Hulkkonen T, Hillamo H, Sarjovaara T, Larmi M. Experimental study of spray characteristics between hydrotreated vegetable oil (HVO) and crude oil based EN 590 diesel fuel. SAE Technical Paper 2011–24-0042, 2011..
[8] Bohl T, Smallbone A, Tian G, Roskilly AP. Particulate number and NOx trade-off comparisons between HVO and mineral diesel in HD applications. Fuel 2018;215:90–101.
[9] Cheng Q, Tuomo H, Kaario OT, Martti L. Spray dynamics of HVO and EN590 diesel fuels. Fuel 2019;245:198–211.
[10] Kuronen M, Mikkonen S, Aakko P, Murtonen T. Hydrotreated vegetable oil as fuel for heavy duty diesel engines. SAE Technical Paper 2007–01-4031, 2007..
[11] Vo C, Charoenphonphanich C, Karin P, Susumu S, Hidenori K. Effects of variable O2 concentrations and injection pressures on the combustion and emissions characteristics of the petro-diesel and hydrotreated vegetable oil-based fuels under the simulated diesel engine condition. J Energy Inst 2018;91(6):1071–84.
[12] Alkhayat SA, Joshi GD, Henein N. Analysis and Correlation of Ignition Delay for Hydrotreated Vegetable Oil and Ultra Low Sulfur Diesel and Their Blends in Ignition Quality Tester. Fuel 2021;289:119816. https://doi.org/10.1016/j.fuel.2020.119816.
[13] Marasri S, Ewphun P-P, Srichai P, Charoenphonphanich C, Karin P, Tongroon M, et al. Combustion characteristics of hydrotreated vegetable oil-diesel blends under EGR and low temperature combustion conditions. Int J Automot Technol 2019;20(3):569–78.
[14] Nylund N-O, Erkkilä K, Ahtiainen M, Murtonen T, Saikkonen P, Amberla A, et al. Optimized usage of NExBTL renewable diesel fuel. OPTIBIO. 2011.
[15] Erkkilä K, Nylund N-O, Hulkkonen T, Tilli A, Mikkonen S, Saikkonen P, et al. Emission performance of paraffinic HVO diesel fuel in heavy duty vehicles. SAE Technical paper 2011–01-1966, 2011..
[16] Makinen R, Nylund N-O, Saikkonen P, Amberla A. Bus fleet operation on renewable paraffinic diesel fuel. SAE Technical Paper 2011–01-1965, 2011..
[17] Aatola H, Larmi M, Sarjovaara T, Mikkonen S. Hydrotreated Vegetable Oil (HVO) as a Renewable Diesel Fuel: Trade-off between NO_x, Particulate Emission, and Fuel Consumption of a Heavy Duty Engine. SAE Int J Engines 2009;1(1):1251–62.
[18] Hartikka T, Kuronen M, Kiiski U. Technical performance of HVO (hydrotreated vegetable oil) in diesel engines. SAE Technical Paper 2012–01-1585, 2012..
[19] Sugiyama K, Goto I, Kitano K, Mogi K, Honkanen M. Effects of hydrotreated vegetable oil (HVO) as renewable diesel fuel on combustion and exhaust emissions in diesel engine. SAE Int J Fuels Lubr 2012;5(1):205–17.
[20] Wu Y, Ferns J, Li H, Andrews G. Investigation of combustion and emission performance of hydrogenated vegetable oil (HVO) diesel. SAE Int J Fuels Lubr 2017;10(3):895–903.
[21] Bortel I, Vávra J, Takáts M. Effect of HVO fuel mixtures on emissions and performance of a passenger car size diesel engine. Renewable Energy 2019;140:680–91.
[22] Suarez-Bertoa R, Kousoulidou M, Clairotte M, Giechaskiel B, Nuottimäki J, Sarjovaara T, et al. Impact of HVO blends on modern diesel passenger cars emissions during real world operation. Fuel 2019;235:1427–35.
[23] Ezzitouni S, Soriano JA, Gómez A, Armas O. Impact of injection strategy and GTL fuels on combustion process and performance under diesel engine start. Fuel 2017;200:529–44.
[24] Mikulski M, Hunicz J, Vasudev A, Rybak A, Gęca M. Combustion of Hydrotreated Vegetable Oil in a Diesel Engine: Sensitivity to Split Injection Strategy and Exhaust Gas Recirculation. *ASME 2020 Internal Combustion Engine Division Fall Technical Conference*. American Society of Mechanical Engineers Digital Collection. 2020.
[25] Liu D, Ghafourian A, Xu H. Phenomenology of EGR in a light duty diesel engine fuelled with hydrogenated vegetable oil (HVO), used vegetable oil methyl ester (UVOME) and their blends. SAE Technical Paper 2013–01-1688, 2013..
[26] Dimitriadis A, Seljak T, Vihar R, Žvar Baškovič U, Dimaratos A, Bezergianni S, et al. Improving PM-NOx trade-off with paraffinic fuels: A study towards diesel engine optimization with HVO. Fuel 2020;265:116921. https://doi.org/10.1016/j.fuel.2019.116921.
[27] Lehto K, Elonheimo A, Hakkinen K, Sarjovaara T, Larmi M. Emission reduction using hydrotreated vegetable oil (HVO) with miller timing and EGR in diesel combustion. SAE Int J Fuels Lubr 2012;5(1):218–24.
[28] Heikkilä J, Happonen M, Murtonen T, Lehto K, Sarjovaara T, Larmi M, et al. Study of Miller timing on exhaust emissions of a hydrotreated vegetable oil (HVO)-fueled diesel engine. J Air Waste Manag Assoc 2012;62(11):1305–12.
[29] Hunicz J, Matijošius J, Rimkus A, Kilikevičius A, Kordos P, Mikulski M. Efficient hydrotreated vegetable oil combustion under partially premixed conditions with heavy exhaust gas recirculation. Fuel 2020;268:117350. https://doi.org/10.1016/j.fuel.2020.117350.
[30] Omari A, Pischinger S, Bhardwaj OP, Holderbaum B, Nuottimäki J, Honkanen M. Improving engine efficiency and emission reduction potential of HVO by fuel-specific engine calibration in modern passenger car diesel applications. SAE Int J Fuels Lubr 2017;10(3):756–67.
[31] Shukla PC, Shamun S, Gren L, Malmborg V, Pagels J, Tuner M. Investigation of Particle Number Emission Characteristics in a Heavy-Duty Compression Ignition Engine Fueled with Hydrotreated Vegetable Oil (HVO). SAE Int J Fuels Lubr 2018;11(4):495–505.
[32] Hunicz J, Krzaczek P, Gęca M, Rybak A, Mikulski M. Comparative study of combustion and emissions of diesel engine fuelled with FAME and HVO. Combustion Engines 2021;184(1):72–8.
[33] Kasprzyk P, Hunicz J, Rybak A, Gęca MS, Mikulski M. Excess air ratio management in a diesel engine with exhaust backpressure compensation. Sensors 2020;20(22):6701.
[34] Hohenberg GF. Advanced approaches for heat transfer calculations. SAE Trans 1979:2788–806.
[35] Kline S, McClintock F. Describing uncertainties in single-sample experiments. Engng: Mech; 1953.
[36] Kamiński M, Budzyński P, Hunicz J, Józwik J. Evaluation of changes in fuel delivery rate by electromagnetic injectors in a common rail system during simulated operation. Eksploatacja i Niezawodność 2021;23(2):352–8.
[37] Refaat AA. Correlation between the chemical structure of biodiesel and its physical properties. Int J Environ Sci Technol 2009;6(4):677–94.
[38] Hunicz J, Mikulski M, Koszałka G, Ignaciuk P. Detailed analysis of combustion stability in a spark-assisted compression ignition engine under nearly stoichiometric and heavy EGR conditions. Appl Energy 2020;280:115955. https://doi.org/10.1016/j.apenergy.2020.115955.
[39] Mikulski M, Balakrishnan PR, Hunicz J. Natural gas-diesel reactivity controlled compression ignition with negative valve overlap and in-cylinder fuel reforming. Appl Energy 2019;254:113638. https://doi.org/10.1016/j.apenergy.2019.113638.
[40] Cheng AS (Ed), Upatnieks A, Mueller CJ. Investigation of fuel effects on dilute, mixing-controlled combustion in an optical direct-injection diesel engine. Energy Fuels 2007;21(4):1989–2002. https://doi.org/10.1021/ef0606456.